



HHS Public Access

Author manuscript

Med Eng Phys. Author manuscript; available in PMC 2015 September 17.

Published in final edited form as:

Med Eng Phys. 2014 July ; 36(7): 831–841. doi:10.1016/j.medengphy.2014.03.007.

Analysis of the effects of surface stiffness on the contact interaction between a finger and a cylindrical handle using a three-dimensional hybrid model

John Z. Wu*, Ren G. Dong, Christopher M. Warren, Daniel E. Welcome, and Thomas W. McDowell

National Institute for Occupational Safety and Health, Morgantown, WV, USA

Abstract

Contact interactions between the hand and handle, such as the contact surface softness and contact surface curvature, will affect both physical effort and musculoskeletal fatigue, thereby the comfort and safety of power tool operations. Previous models of hand gripping can be categorized into two groups: multi-body dynamic models and finite element (FE) models. The goal of the current study is to develop a hybrid FE hand gripping model, which combines the features of conventional FE models and multi-body dynamic models. The proposed model is applied to simulate hand-gripping on a cylindrical handle with covering materials of different softness levels. The model included three finger segments (distal, middle, and proximal phalanxes), three finger joints (the distal interphalangeal (DIP), proximal interphalangeal (PIP), and metacarpophalangeal (MCP) joint), and major anatomical substructures. The model was driven by joint moments, which are the net effects of all passive and active muscular forces acting about the joints. The finger model was first calibrated by using experimental data of human subject tests, and then applied to investigate the effects of surface softness on contact interactions between a finger and a cylindrical handle. Our results show that the maximal compressive stress and strain in the soft tissues of the fingers can be effectively reduced by reducing the stiffness of the covering material.

* Corresponding author at: NIOSH/CDC, 1095 Willowdale Road, MS-2027, Morgantown, WV 26505, USA. Tel.: +1 304 285 5832; fax: +1 304 285 6265. jwu@cdc.gov (J.Z. Wu)..

Publisher's Disclaimer: This article appeared in a journal published by Elsevier. The attached copy is furnished to the author for internal non-commercial research and education use, including for instruction at the authors institution and sharing with colleagues.

Publisher's Disclaimer: Other uses, including reproduction and distribution, or selling or licensing copies, or posting to personal, institutional or third party websites are prohibited.

Publisher's Disclaimer: In most cases authors are permitted to post their version of the article (e.g. in Word or Tex form) to their personal website or institutional repository. Authors requiring further information regarding Elsevier's archiving and manuscript policies are encouraged to visit: <http://www.elsevier.com/authorsrights>

Disclaimers

The findings and conclusions in this report are those of the authors and do not necessarily represent the views of the National Institute for Occupational Safety and Health.

Ethical approval: Study protocol "Evaluation of Equipment and Methodologies Used in the Assessment of Hand-Transmitted Vibration Exposure" (ID: 06-HELD-02XP) was approved by NIOSH HSRB (Human Subjects Review Board, National Institute for Occupational Safety and Health).

Conflict of interest: None declared.

Keywords

Hand; Fingers; Handle; Multi-body dynamics; Finite element model; Soft tissues

1. Introduction

Musculoskeletal disorders of the hand and fingers are associated with occupational activities across all industrial sectors [1]. Since the handle serves as an interface between an operator and a machine or a tool, it is well accepted that an optimized design of the handle can reduce both physical effort and musculoskeletal fatigue, thereby improving comfort and reducing the risk of musculoskeletal disorders. Previous experimental studies indicate that grip strength, operator's comfort, and safety depend on the handle diameter [2–6], the properties of the surface materials [7,8], the handle shape [9,10], the friction of the contact surface [11], the stiffness of the contact surface [12], and also the posture of the operator [13]. It is difficult to objectively evaluate the biomechanical responses of the hand-arm system to the variations of the operating conditions in experiments because the forces in the musculoskeletal system cannot be easily measured *in vivo*. Therefore, biomechanical models of the system become essential tools for exploring the mechanical loading environment associated with injury mechanisms.

Researchers have developed multiple models of the hand and fingers for simulating different problems. Brook et al. [14] developed a biomechanical model of the dynamics of the index finger and applied their model to simulate the muscle forces in pinch grip and disc rotation. Biggs and Horch [15] proposed a three-dimensional (3D) kinematic long finger model and qualitatively validated their model via experimental data of tendon/muscle excursions for the motion of the MCP joint. Valero-Cuevas et al.'s [16] finger models included anatomically realistic tendon/muscle connections and musculoskeletal parameters. The whole-hand models proposed by Sancho-Bru et al. [17,18] were used to simulate the muscle loading for static gripping and free movements. Freund et al. [19] developed a hand model to investigate the dependence of the fingertip contact force on the gripping force, handle diameter, and hand size. All these hand models are multi-body dynamical models, in which the fingers are simulated using linkage systems composed of rigid finger segments linked by joints and connected by muscle/tendon units. Since these models do not contain passive soft tissues (i.e., skin and subcutaneous tissues), they cannot be applied to simulate the contact interactions between the fingers and objects, which are important for some practical problems.

For ergonomic designs of tool handles, it is important to understand the contact mechanics between the hand and handle, such as the effects of the contact surface softness and contact surface curvature on the comfort of the operators. The contact condition is known to be one of the essential factors that determine vibration resonance characteristics [20]. Therefore, hand contact mechanics are also important for understanding the biodynamic responses of the hand-arm system and to explore the mechanisms of hand-arm vibration syndrome [20,21]. Although contact pressures between the hand and a hard surface can be measured reliably using pressure sensor film, the same technique cannot be applied to evaluate the

mechanics of the hand/handle contact. Since handles are typically covered with soft materials, which are usually much softer than the pressure sensor film, inserting the pressure sensor film between the hand and the handle will substantially alter the contact mechanics. Consequently, finite element (FE) models have been developed to examine contact conditions for such problems. Previously, we have proposed FE models to study the dynamic contact between a fingertip and a flat plate [22], the effects of the curvature of the contact surface on contact pressures [23], and the contact interactions between a fingertip and a vibrating plate [24]. In all these previous FE models, only one fingertip segment was included, and the simulations were driven by directly applying contact force or displacement. The contact force was prescribed as a model input and it was not related to the joint torques or muscle forces of the hand-arm in these models.

The goal of the current study is to develop a hybrid finger model to simulate hand gripping on a cylindrical handle with soft covering materials. The hybrid finger model will combine the features of the conventional FE models and the multi-body dynamic models; it includes three finger segments (distal, middle, and proximal phalanges), three joints [the distal interphalangeal (DIP), proximal interphalangeal (PIP), and metacarpophalangeal (MCP) joint], and contains the major anatomical substructures of the finger (i.e., soft tissues, nail, and bone). The model will be driven by the joint moments, which are net effects of passive and active forces (due to the effects of the connective tissues, ligaments, tendons, and muscles) acting about the joints. In this study, the proposed model is applied to investigate the effects of the softness of the contact surface on the contact interactions between a finger and a cylindrical handle.

2. Methods

2.1. Finite element model

The proposed 3D FE model of the grip features a finger and a cylindrical handle, as illustrated in Fig. 1. The FE model was developed to simulate a middle finger, which consists of a distal, a middle, and a proximal phalanx (Fig. 1B). The finger model included soft tissues, bone, and nail. External shapes of all three finger segments were considered to be rotationally symmetrical. The middle and proximal phalanges were conical frustums, whereas the distal phalanx was a conical frustum connected with a hemispherical-like fingertip. The dimensions of the finger segments were adjusted to match the average of all subjects. The dimensions of the bony cross-sections were determined based on published experimental measurements [25].

The DIP and PIP joints were modeled as hinges with one degree of freedom (DOF, flexion/extension). The MCP joint was modeled as a universal joint with two DOFs (flexion/extension and adduction/abduction) (Fig. 1B); however, the DOF in adduction/abduction has been constrained in the study. The proximal phalanx is linked to ground via the MCP joint. The system is mechanically equivalent to the case where a metacarpal bone is fixed in space. In the current problem, all finger joints exhibited rotational motions only around the z -axis (the motion of adduction/abduction in the MCP joint was constrained). The finger joints were built on the apices of the bony segments. Each apex was constrained by the end surface of the corresponding bony segment.

The soft tissues were considered to be connected to the side surfaces of the bony segments. The effects of the passive stiffness due to the deformation of the soft tissues around the joint creases were neglected, i.e., the ends of the finger segments could penetrate into each other without resistance. The contact pairs were built between the external surface of the cylinder covering and the external side surfaces of the finger segments. The friction coefficient between the skin/cylinder contact interface was considered to be 0.30 [26,27]. The FE model is geometrically nonlinear to cope with large deformation. The FE model was developed using a commercial software package ABAQUS.

For all simulations of cylinders with or without soft covering materials, the external diameter of the cylinder was 40 mm. The cylinder was of aluminium and was considered to be covered with three different materials (thickness 1.5 mm): synthetic viscoelastic urethane polymers of three different levels of stiffness (Sorbothane with three different hardness: 30, 50, and 70 on an OO durometer scale), which are labeled as “Soft”, “Medium”, and “Hard”, respectively. The material properties of the Sorbothanes were evaluated in unconfined compressive tests, as described in detail in Appendix. The obtained stress–strain curves have been fitted to two-term Mooney–Rivlin constitutive models. The bone and nail are assumed to be linearly elastic whereas the soft tissues were considered as nonlinearly elastic. The mechanical properties of the bone, nail, and soft tissues have been described in our previous studies [28,29].

2.2. Experimental set-up and test procedure

Grip tests were accomplished by using an instrumented cylindrical handle (external diameter 40 mm and length 200 mm), as illustrated in Fig. 2A. To eliminate the effects of pushing or pulling forces, the handle was suspended vertically with a string. The height of the handle was adjusted to approximately the height of each subject's waist, facilitating a comfortable grip.

The instrumented handle was made of aluminium and featured two built-in force transducers (Interface, SML-50) to measure the grip force (F_N) (Fig. 2B). The grip force was displayed on a monitor, helping subjects maintain the desired force level. The distributions of the contact pressure between the fingers and handle were measured by using a pressure sensor film (TekScan Model 5076, 345 kPa range) that was wrapped around the surface of the handle (Fig. 2A). The pressure sensor film (dimension of 80 mm × 80 mm) contained a 42 × 42 array of sensors, such that it resulted in a spatial resolution of 1.9 mm × 1.9 mm. We only measured the contact pressure on four fingers due to the size limitation of the pressure sensor film. The gripping position of the hand on the cylinder was carefully checked to keep the fingertips about three to four cells (about 6–8 mm) from the boundary of the pressure sensor film for the unloaded state, such that the finger/cylinder contact region was at least one cell away from the mat boundary under the maximal grip condition (Fig. 2A and B). Subjects' fingers were approximately perpendicular to the cylinder axis, and the subjects' wrists maintained a neutral posture during the gripping test (Fig. 2A). The location of the fingertips was aligned with the edge of the handle segment (Fig. 2B).

The pressure sensor film was calibrated by comparing the contact pressure measurements with those obtained via the force transducers built in the handle. The grip force (F_N) is

mechanically equivalent to the mathematical integration of contact pressure over half of the cylinder surface: $F_N = \int_0^\pi \int_0^L p(\theta, z) \sin(\theta) r dz d\theta$ (Fig. 2B), with p , L , r , θ , and z being the contact pressure, cylinder length, cylinder radius, and integration variables, respectively.

A total of ten subjects (5 male and 5 female; age 25 *SD* 7 years) participated in the tests, following informed consent approved by the NIOSH Human Subjects Review Board. The subjects were either students or office workers. All subjects were right-handed and only the right hands were used in the tests. The subjects were instructed to first gently grip the handle and slowly increase the grip force until it (F_N) reached a specified loading level (5 N, 10 N, 20 N, 40 N, 60 N, and 80 N). The tests were performed using only the handle without soft covering materials. At each of the loading levels, the subjects were instructed to keep the grip force constant for 10 s and then to completely release. The subjects relaxed for about 30 s before they performed tests at the next, randomized grip force level. The test protocol was designed to minimize the “memory” effects of the pressure sensor film. All test trials were repeated three times. The contact pressure and the grip force data were collected at a rate of 10 Hz. In order to eliminate noise and fluctuations, the measured data were averaged over a time period of 10 s, during which the subjects maintained a constant grip force.

2.3. Model calibration and simulation

In this study, we applied a dynamic FE model to simulate the quasi-static gripping. The FE simulations were performed in a forward dynamic scheme – the joint moments were applied, whereas the finger joint angular motions and the deformation and stress/strain of the soft tissues are predicted. The joint moments were assumed to increase gradually from zero, such that the effects of the mass inertia of the finger segments will be negligible. In order for the modeling to be comparable to the experiments, which were performed under static conditions, the simulations have to be performed in such a manner that the dynamic forces associated with the effects of the mass inertia are negligible. The magnitude ratio of the moments in the three joints was assumed to be constant during loading. The joint moments were applied in small increments; the entire loading was accomplished over 200 incremental steps. The model variables were output for every incremental step during the loading process such that the entire grip force range of the experiments was simulated.

The purpose of the model calibration calculations was to determine an optimized joint moment ratio such that the predicted contact pressure distributions achieve the best fit to the experimental measurements. Based on our previous analysis [30], the ratio of the moments applied at the DIP, PIP, and MCP joints was initially assumed to be 1.00:3.75:5.52. The DIP joint moment was held constant, whereas the PIP and MCP joint moments were varied by $\pm 30\%$ in steps of 10% around the initial values, until the predicted contact pressures matched the average of the data obtained from all subjects. The ratio of the joint moments was kept constant, as the joint moments increased as a function of time during each of the individual numerical tests. In the calibration computations, the cylinder was assumed to be covered with a thin, hard plastic material, which mimicked the experimental conditions.

In the model predictions, the cylinder was considered to be wrapped with materials of three different levels of stiffness, and the effects of the covering materials on the contact

mechanics were calculated. It was further assumed that the gripping effort was independent of the cylinder covering, and the joint moment ratio was the same as for the case of gripping on the bare cylinder handle. The optimized ratio of the moments in the DIP, PIP, and MCP joints was applied in the calculations. The effects of the covering materials were evaluated by comparing the contact pressures and the stress/strain in the soft tissues when gripping the cylinders covered with different materials. The joint moments were increased to the magnitudes to reproduce the representative contact pressures observed in our experiments.

3. Results

3.1. Experimental data and model calibrations

The average contact pressure distributions on the cylinder surface for four different grip force levels (5 N, 10 N, 20 N, and 40 N), as observed in the experiments, are shown on the left column of Fig. 3. These measurements were utilized for the model calibrations.

The contact pressure on four fingers is illustrated in Fig. 3. It is seen that the majority of the grip force was contributed by the index, middle, and ring fingers (Fig. 3, left column); and the contact force distributions on these three fingers varied with the increase in grip force. The measured contact pressures on the middle finger were more reliable (framed by red boxes in Fig. 3, left column), because they were less affected by conditions of the pressure sensor's boundary.

The ratio of the maximal contact pressure at the distal, middle, and proximal segment of the middle finger is 1:0.89 (SD 0.27):0.72 (SD 0.30) (Fig. 4). Although the pattern of the contact pressure distributions of the fingers was different from subject to subject, general trends of the pressure distribution on each segment of a finger were consistent: the contact pressure on the distal segment was substantially greater than those of the middle and proximal segments.

Our analysis indicated that the best fit of the predicted contact pressure distributions (i.e., the peak contact pressure values at the distal, middle, and proximal segments) to the experimental data was achieved by applying an optimized moment ratio of 1.00:2.63:5.52 at the DIP, PIP, and MCP joints. The calculated contact pressure distributions are shown in Fig. 3 (right column) in comparison with the corresponding experimental data (Fig. 3, left column). The calculated maximal contact pressures at the distal, middle, and proximal finger segments for different contact force levels are listed in Table 1. Our results show that calculated pressure distributions match approximately the experimental data for the entire observed grip force range. The resolution for the contact pressure values at the middle and proximal regions of the experimental data (Fig. 3, left) was poor, and the values were estimated.

The model shows distinct contact areas for the distal, middle, and proximal regions for all grip force levels, while the contact areas cannot be determined clearly in the measured data. The simulation results show that the increase of the grip force from 5 N to 40 N causes increases in the contact pressure by about six times, but results in little increase in the contact area (<2 %) (Fig. 3, right).

The variations of the joint moment as a function of time are illustrated in Fig. 5. The joint loadings were applied within a time period of 0.5 s; and the ratio of the joint moments was kept constant during the loading. The distributions of the maximal tissue compressive stress on the finger skin surface and the maximal compressive tissue strains are shown in the left and right columns of Fig. 6, respectively. The compressive and tensile stress (strain) values are represented by negative and positive signs, respectively.

3.2. Model prediction

The maximal contact pressure was approximately proportional to the grip force for $F_N = 10$ N (Fig. 3, right column): the maximal contact pressure at the distal fingertip increased from 100 kPa to 390 kPa when the grip force increased from 10 N to 40 N. The magnitude of the maximal compressive stress increased about four times from -0.10 MPa to -0.43 MPa (Fig. 6, left column), while the magnitude of the maximal compressive strain increased only about 38% from -0.64 to -0.88 (Fig. 6, right column), when the grip force increased from 10 N to 40 N. This is due to the nonlinearity of the soft tissue materials and the three-dimensional constrain conditions of the tissues in the contact regions. The magnitude of the maximal compressive stress in the fingertip soft tissue (Fig. 6, left) was slightly greater than the corresponding maximal contact pressure (Fig. 3, right), as expected. The maximal compressive tissue stress/strain was observed in the distal segment, whereas the minimal compressive stress/strain was in the middle segment (Fig. 6). The distribution of the maximal compressive strain across the tissue thickness tended to become more uniform with increasing grip force.

For a given gripping effort, which approximately corresponds to grip force level of 20 N, the contact pressure decreased with decreasing stiffness of the covering material (Fig. 7). The maximal contact pressure decreased from 200 kPa to 170 kPa, a reduction of 15% when the covering material varied from “Hard” to “Soft”. The change in material stiffness did not alter the pattern of the contact pressure distributions. The optimized joint moment ratio obtained in the model calibrations was used in the prediction.

The effects of the covering stiffness on the contact conditions between the fingers and the cylinder were manifested more clearly in tissues' strain and stress in each finger segment, as shown in Figs. 8 and 9, respectively. Our results show that the maximal compressive stress on the skin surface of the distal, middle, and proximal segments decreased from 220 kPa, 96 kPa, and 110 kPa to 180 kPa, 88 kPa, and 95 kPa, respectively, when the stiffness of the covering material decreased from “Hard” to “Soft” (Fig. 8). The corresponding distributions of the maximal compressive strains on the skin surfaces of the finger segments are shown in Fig. 9. When the stiffness of the covering material decreased from “Hard” to “Soft” (Fig. 9), the magnitude of the maximal compressive strain on the distal, middle and proximal segments decreased from 0.76, 0.59, and 0.62 to 0.71, 0.57, and 0.59, respectively.

Furthermore, we have quantified the contact areas on the distal, middle, and proximal finger segments for different contact stiffness for the simulations, as shown in Figs. 8 and 9, and found that the contact area increased by 8% and 14%, when the covering material is changed from “Hard” to “Medium” and from “Hard” to “Soft” (Fig. 9), respectively. The greatest increase in the contact area was observed at the middle and proximal finger segments, where

the contact area increased by around 20% and 16%, respectively, whereas the contact area at the distal segment increased by only 6% when the stiffness of the covering material decreased from “Hard” to “Soft”.

4. Discussion

Our study suggests that the maximal compressive stress on the skin surface of the middle finger can be reduced by reducing the stiffness of the material covering a cylindrical handle. The current simulation results indicate that the maximal compressive stresses on the distal, middle, and proximal segments were reduced by 18.2%, 8.3%, and 13.6%, respectively, when the stiffness of the covering material decreased from “Hard” to “Soft” (Fig. 8). Our results suggest that an operator's comfort may be effectively modulated by varying the stiffness of the covering materials, since the comfort of a finger may be associated with the responses of the mechanoreceptors that sense stress/strain states in their surrounding tissues [31,32]. Our observations may generally support the practice whereby tool handles are often wrapped with a layer of soft materials to improve comfort.

In the current study, we demonstrated that decreasing the stiffness of the materials covering a cylindrical handle will generally decrease the stresses and strains in the soft tissues. For practical applications, however, the stiffness of the covering materials can only be varied within a certain range. A covering material that is too soft could make a power tool difficult to control, especially for a vibrating tool [33,34]. Consequently, the operators may need to apply more force to grasp the tool, resulting in an increase of the musculoskeletal load in the hand. This is similar to scenarios of power tool operations while wearing thick gloves [35]. From a dynamical point-of-view, a reduction of the contact stiffness may change the resonant frequencies of the fingers and the hand-arm system and reduce the transmitted vibration at frequencies above the resonant frequencies [20]. This may increase the hand's exposure to vibration, if the altered resonances fall within the range of the tools' dominant vibration frequencies. Therefore, there should exist an optimized contact stiffness for a tool handle, which is dependent on the functions and dynamic characteristics of the tool. The model developed in the current study provides a preliminary biomechanical foundation for the optimization analysis and design of tool handles.

It is interesting to note that a covering material's stiffness affects tissue strain differently than tissue stress. A comparison of the stress (Fig. 8) and strain (Fig. 9) distributions indicated that reducing the stiffness of the covering material caused a reduction of tissue stress by 8.3–18.2%, whereas it induced a reduction of tissue strain by merely 3.3–6.5%. This inconsistency in the dependencies of tissue stress and strain on a covering material's stiffness is likely due to the nonlinearity of the soft tissues and the covering materials and relative thickness of materials involved. Soft tissues and polymers typically exhibit highly nonlinear mechanical behavior; their stiffness typically increases with increasing deformation, as illustrated in Fig. A.1. Consequently, very small variations in strain will result in very great variations in stress at large deformations. This is best demonstrated at the distal segment, where the soft tissues experienced very large deformation (maximal compressive strain 71–76%) and the maximal compressive stress varied by as much as 18.2% whereas the maximal compressive strain varied merely 6.5% (Figs. 8–9).

The joint angular motions are coupled with the grip force, the finger deformations, and the contact stiffness. In the forward dynamic analysis, these coupling effects are considered. The joint angular variation due to the variations in the grip force and covering materials was observed to be very small and negligible compared to those associated with other variations in the experimental condition. In the current study, the maximal joint angular change between two extreme scenarios with the largest and smallest tissue deformations (i.e., 40 N grip force combined with soft covering material vs. 5 N grip force combined with hard covering material) was smaller than 1 °.

The ratio of the maximal contact pressure of the distal, middle, and proximal finger segment (Fig. 4) observed in our study is consistent in trend with Chao et al's [36] results, who measured the ratio of the contact forces applied on the distal, middle, and proximal segments in grip. Because the maximal contact pressure is associated with the contact force on each finger segment, the results of these two studies should be comparable, at least in trend.

One limitation of the current simulation is that the ratio of the moments applied in the DIP, PIP, and MCP joints is assumed to be constant. The reliable agreement between calculated contact pressure and the experimental measurements over the entire grip force range suggests that the assumption of the constant joint moment ratio is reasonable. This assumption may not be strictly correct physiologically since people may tend to grip in a manner to minimize the grip effort for different gripping force levels, resulting in varying joint moment ratios as a function of the gripping force [37]. The joint moment ratio in fingers is subject specific and may also be dependent on the contact stiffness [38]. In addition, the dimensions of the handle may alter a person's gripping behaviors. However, the stiffness of the handle covering material is much higher than that of the soft tissues and typical handle diameters are around 40 mm, based on previous ergonomic studies [5,8,38]. Indeed, the adjustment of the joint moment ratio for different gripping force levels was observed to be so minor that they did not produce measurable contact pressure variations, at least in the current measurements using a pressure sensor film. The effects of the contact stiffness and handle dimensions on the ratio of the joint moments should be more precisely analyzed in the future.

One of the limitations of the proposed finger model was that the soft tissues surrounding the joints were not included. Consequently, the predicted contact pressure distributions on the cylindrical surface show three separate regions that are due to the contacts of the distal, middle, and proximal segments. In practical cases, the contact regions of the distal, middle, and proximal segments may be interconnected because of the contact between the cylinder and the soft tissues surrounding the joints. We observed in the experiments (Fig. 3) that the contact pressure of the tissues surrounding the joints on the cylinder is small and is not measurable using the pressure sensor film. Therefore, it is reasonable to neglect the contribution of the tissues surrounding the joints to the contact interactions.

Because of the technical limitations in measurement, the simulated contact pressure cannot be compared precisely with that observed in the experiments. The calculated contact pressures are continuous in space at the contact surface, whereas the measured contact pressures are discrete at the contact surface. This is because pressure reading within a cell

(1.9 mm × 1.9 mm) is constant and it represents the average value at that cell; and there exists sudden variation in pressure values between two neighboring cells. Although this type of the pressure sensor is the best currently available, the spatial resolution of 1.9 mm is pretty large relative to the finger dimension. A further problem is that the sensitive range of the sensor is quite narrow; the pressure sensor film will become saturated or not responsive if the pressure is above or below the effective range, respectively.

In summary, we developed a novel finger model to simulate a hand gripping a cylindrical handle. The proposed model differs from previous finger models in that it combines conventional FE models with multi-body dynamic models, such that both detailed stress/strain distributions in the soft tissues and the global kinetics of the fingers can be simulated. We have calibrated the model using experimental data, and applied the model to investigate the effects of the stiffness of the contact surface on the contact mechanics between the finger and a cylindrical handle.

Acknowledgement

We would like to thank Dr. Frank Buczek (National Institute for Occupational Safety and Health) for the critical review and numerous suggestions, which helped us to improve the manuscript.

Funding: None.

Appendix

Three synthetic viscoelastic urethane polymers (Sorbothane Inc., Kent, OH, USA) of different stiffness measures (specified as specimens S, M, and H) were selected for the handle covering. The mechanical properties of the polymers were tested via unconfined compressions. The specimens of the covering materials were compressed between two smooth cylindrical platens, while the lateral side of the specimens were free to expand during the compressions. The cylindrical probes were cut from raw material sheets using a steel punch, which has an outside level and a sharp edge. The probes had a diameter of approximately 5.99 mm. The heights of the probes were 4.79, 3.29, and 3.77 mm, respectively, for the S (Soft), M (Medium) and H (Hard) specimens. A micro-mechanical test machine (Model: Mach-1, Biomomentum Inc., Laval, QC, Canada) was utilized for the material testing. The testing machine was equipped with a displacement sensor with a resolution of 0.5 μm and a 98 N (10 kg) load cell with a resolution of 2.45 mN (250 mg). The compressions were performed at a very slow rate (0.01 mm/s), such that the materials' viscous effects were negligible. The stress–strain curves of these three polymer specimens are shown in Fig. A.1. Two-term Mooney–Rivlin models were applied to fit the stress–strain curves. The probe dimensions and material parameters are listed in Table A.1.

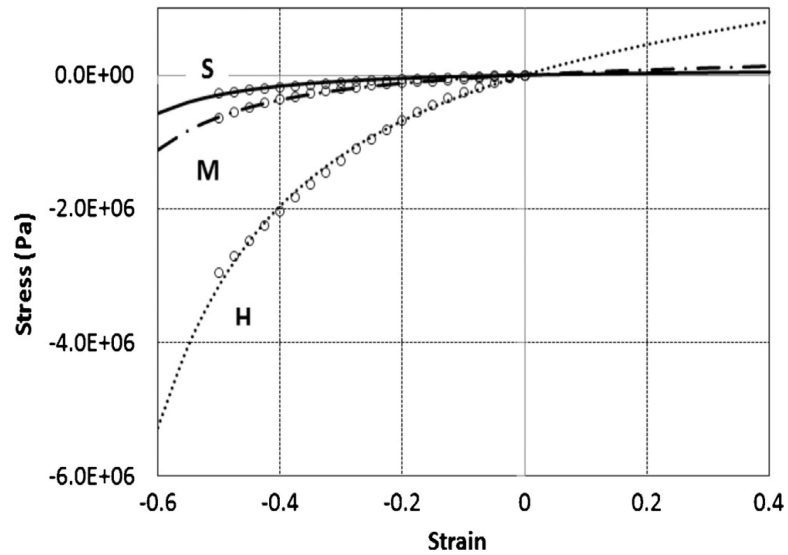


Fig. A.1. Stress–strain curves of three different covering materials. The covering materials labeled with “S” (Soft), “M” (Medium), and “H” (Hard) are synthetic viscoelastic urethane polymers (Sorbothane Inc., Kent, OH, USA) with a hardness of 30, 50, and 70, respectively, on an OO durometer scale.

Table A.1

Probe dimensions and mechanical parameters for the covering materials “S” (Soft), “M” (Medium), and “H” (Hard). Two-term Mooney-Rivlin models were applied to fit the stress-strain curves shown in Fig. A.1. C01 and C10 are the material parameters of Mooney-Rivlin model.

Specimens	Dimension		Material parameters	
	Diameter (mm)	Height (mm)	C10 (Pa)	C01 (Pa)
S	5.99	4.79	14800.8	13613.9
M	5.99	3.29	64492.4	12252.5
H	5.99	3.77	448406.8	563.5

References

1. Marras WS, Cutlip RG, Burt SE, Waters TR. National occupational research agenda (nora) future directions in occupational musculoskeletal disorder health research. *Appl Ergon.* 2009; 40(1):15–22. [PubMed: 18462703]
2. Seo NJ, Armstrong TJ, Ashton-Miller JA, Chaffin DB. Wrist strength is dependent on simultaneous power grip intensity. *Ergonomics.* 2008; 51(10):1594–605. [PubMed: 18803097]
3. Adams SK, Peaterson PJ. Maximum voluntary hand grip torque for circular electrical connectors. *Appl Ergon.* 1990; 21:78–9.
4. Imrhan SN, Farahmand K. Male torque strength in simulated oil rig tasks: the effects of grease-smearred gloves and handle length, diameter and orientation. *Appl Ergon.* 1999; 30:455–62. [PubMed: 10484281]
5. Lee JW, Rim K. Measurement of finger joint angles and maximum finger forces during cylinder grip activity. *J Biomed Eng.* 1991; 13(2):152–62. [PubMed: 2033951]

6. Kong YK, Freivalds A. Evaluation of meat-hook handle shapes. *Int J Ind Ergon.* 2003; 32:13–23.
7. Williams CD. A novel redesign of food scoops in high volume food service organizations. *Work.* 2003; 20(2):131–5. [PubMed: 12671207]
8. Marvik R, Nesbakken R, Lango T, Yavuz Y, Vanhauwaert Bjelland H, Ottermo MV, Stavadahl O. Ergonomic design criteria for a novel laparoscopic tool handle with tactile feedback. *Minerva Chir.* 2006; 61(5):435–44. [PubMed: 17159752]
9. Jenmalm P, Goodwin AW, Johansson RS. Control of grasp stability when humans lift objects with different surface curvatures. *J Neurophysiol.* 1998; 79(4):1643–52. [PubMed: 9535935]
10. Kong YK, Lowe BD, Lee SJ, Krieg EF. Evaluation of handle shapes for screwdriving. *Appl Ergon.* 2008; 39(2):191–8. [PubMed: 17572374]
11. Seo NJ, Armstrong TJ, Chaffin DB, Ashton-Miller JA. The effect of handle friction and inward or outward torque on maximum axial push force. *Hum Factors.* 2008; 50(2):227–36. [PubMed: 18516834]
12. Pheasant S, O'Neill D. Performance in gripping and turning – a study in hand/handle effectiveness. *Appl Ergon.* 1975; 6(4):205–8. [PubMed: 15677185]
13. Fransson C, Winkel J. Hand strength: the influence of grip span and grip type. *Ergonomics.* 1991; 34(7):881–92. [PubMed: 1915253]
14. Brook N, Mizrahi J, Shoham M, Dayan J. A biomechanical model of index finger dynamics. *Med Eng Phys.* 1995; 17(1):54–63. [PubMed: 7704345]
15. Biggs J, Horch K. A three-dimensional kinematic model of the human long finger and the muscles that actuate it. *Med Eng Phys.* 1999; 21(9):625–39. [PubMed: 10699565]
16. Valero-Cuevas FJ, Zajac FE, Burgar CG. Large index-fingertip forces are produced by subject-independent patterns of muscle excitation. *J Biomech.* 1998; 31(8):693–703. [PubMed: 9796669]
17. Sancho-Bru JL, Perez-Gonzalez A, Vergara-Monedero M, Giurintano D. A 3D dynamic model of human finger for studying free movements. *J Biomech.* 2001; 34(11):1491–500. [PubMed: 11672724]
18. Sancho-Bru JL, Perez-Gonzalez A, Vergara M, Giurintano DJ. A 3D biomechanical model of the hand for power grip. *J Biomech Eng.* 2003; 125(1):78–83. [PubMed: 12661199]
19. Freund J, Toivonen R, Takala EP. Grip forces of the fingertips. *Clin Biomech (Bristol, Avon).* 2002; 17(7):515–20.
20. Dong RG, Wu JZ, McDowell TW, Welcome DE, Schopper AW. Distribution of mechanical impedance at the fingers and the palm of the human hand. *J Biomech.* 2005; 38(5):1165–75. [PubMed: 15797597]
21. Dong RG, Wu JZ, Welcome DE. Recent advances in biodynamics of human hand-arm system. *Ind Health.* 2005; 43(3):449–71. [PubMed: 16100922]
22. Wu JZ, Dong RG, Smutz WP, Rakheja S. Dynamic interaction between a fingerpad and a flat surface: experiments and analysis. *Med Eng Phys.* 2003; 25(5):397–406. [PubMed: 12711237]
23. Wu JZ, Dong RG. Analysis of the contact interactions between fingertips and objects with different surface curvatures. *Proc Inst Mech Eng H.* 2005; 219(2):89–103. [PubMed: 15819480]
24. Wu JZ, Krajnak K, Welcome DE, Dong RG. Three-dimensional finite element simulations of the dynamic response of a fingertip to vibration. *J Biomech Eng.* 2008; 130(5):054501. [PubMed: 19045525]
25. Schuler-Ellis FP, Lazar GT. Internal morphology of human phalanges. *J Hand Surg Am.* 1984; 9(4):490–5. [PubMed: 6747232]
26. Zhang M, Mak AF. In vivo friction properties of human skin. *Prosthet Orthot Int.* 1999; 23(2):135–41. [PubMed: 10493141]
27. Savescu AV, Latash ML, Zatsiorsky VM. A technique to determine friction at the fingertips. *J Appl Biomech.* 2008; 24(1):43–50. [PubMed: 18309182]
28. Wu JZ, Herzog W. Analysis of the mechanical behavior of chondrocytes in unconfined compression tests for cyclic loading. *J Biomech.* 2006; 39(4):603–16. [PubMed: 16439231]
29. Wu JZ, Dong RG, Welcome DE. Analysis of the point mechanical impedance of fingerpad in vibration. *Med Eng Phys.* 2006; 28(8):816–26. [PubMed: 16426886]

30. Wu JZ, Dong RG, McDowell TW, Welcome DE. Modeling the finger joint moments in a hand at the maximal isometric grip: the effects of friction. *Med Eng Phys.* 2009; 31(10):1214–8. [PubMed: 19700363]
31. Mountcastle V, LaMotte R, Carli G. Detection thresholds for stimuli in humans and monkeys: Comparison with threshold events in mechanoreceptive afferent nerve fibers innervating the monkey hand. *J Neurophysiol.* 1972; 35:122–36. [PubMed: 4621505]
32. Johansson RS, Vallbo AB. Tactile sensibility in the human hand: relative and absolute densities of four types of mechanoreceptive units in glabrous skin. *J Physiol.* 1979; 286:283–300. [PubMed: 439026]
33. Soechting JF, Flanders M. Sensorimotor control of contact force. *Curr Opin Neurobiol.* 2008; 18(6):565–72. [PubMed: 19081242]
34. White O, Thonnard JL, Wing AM, Bracewell RM, Diedrichsen J, Lefevre P. Grip force regulates hand impedance to optimize object stability in high impact loads. *Neuroscience.* 2011; 189:269–76. [PubMed: 21640167]
35. Wimer B, McDowell T, Welcome D, Warren C, Dong R. Effects of gloves on the grip strength applied to cylindrical handles. *Int J Ind Ergon.* 2010; 50(5):574–83.
36. Chao, EYS.; An, KN.; Cooney, WP., III; Linscheid, RL. Chapter 5: Hand functional strength assessment and its clinical application, *Biomechanics of the Hand.* World Scientific; Singapore/New Jersey/London/Hong Kong: 1989.
37. Flanagan JR, Burstedt MK, Johansson RS. Control of fingertip forces in multidigit manipulation. *J Neurophysiol.* 1999; 81(4):1706–17. [PubMed: 10200206]
38. Wings SA, Eonta SE, Soechting JF, Flanders M. Effects of object compliance on three-digit grasping. *J Neurophysiol.* 2009; 101(5):2447–58. [PubMed: 19279149]

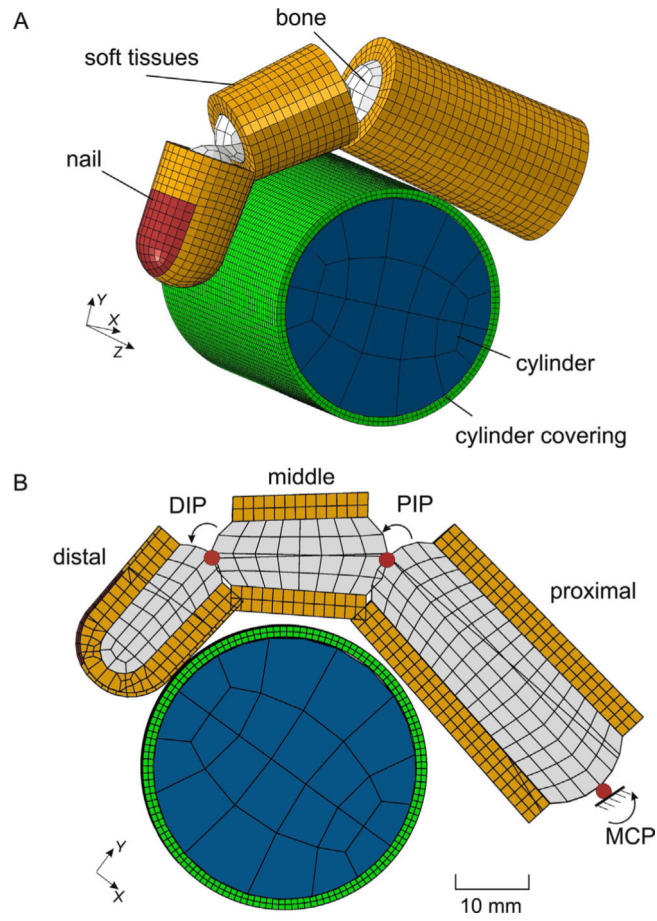


Fig. 1.

Proposed finger model mimicking a gripping task. (A) Three dimensional sketch of the model. (B) Cross-sectional view of the model. The finger model consisted of three segments, i.e., distal, middle, and proximal segments. The finger segments contain three different materials: bone, soft tissues, and nail. In order to simulate the effects of the contact surface stiffness, the cylindrical handle was considered to be covered with different materials. The finger was driven by the moments applied at the DIP, PIP, and MCP joints. The cylinder was fixed at its axial center, and it can rotate around its axis.

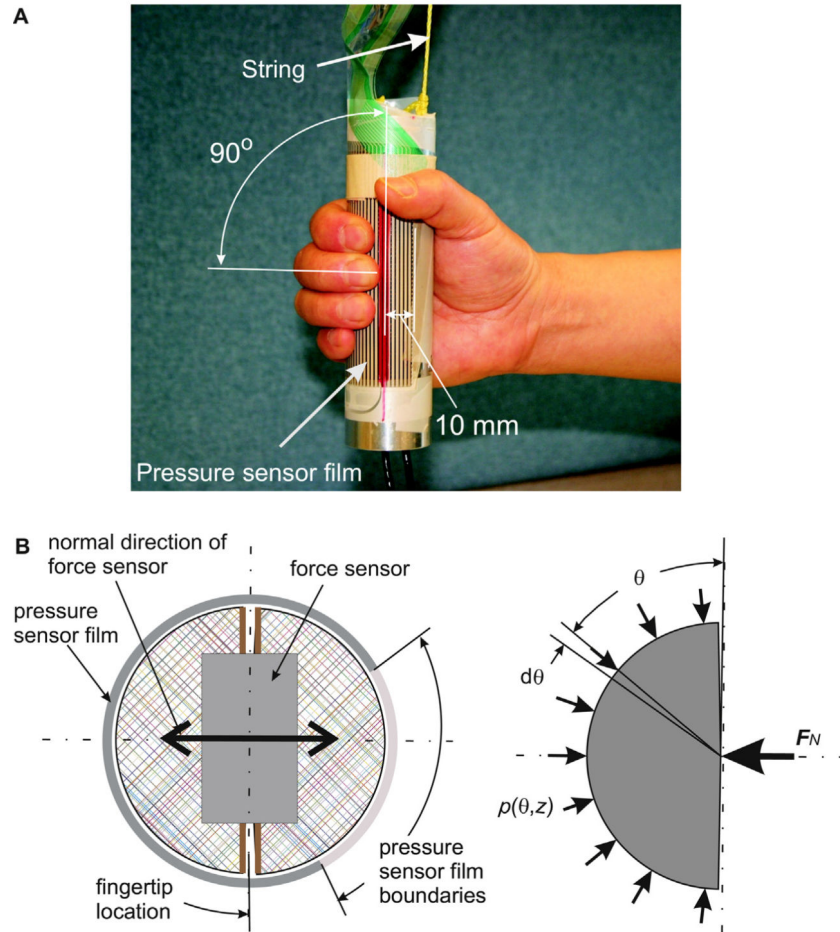


Fig. 2. Experimental tests of the contact pressure. (A) Experimental set-up. (B) Sketch of the determination of gripping force. The contact pressure was measured via a pressure sensor film wrapped on a cylindrical handle. The grip force was estimated by measuring the force via two force transducers built in the handle.

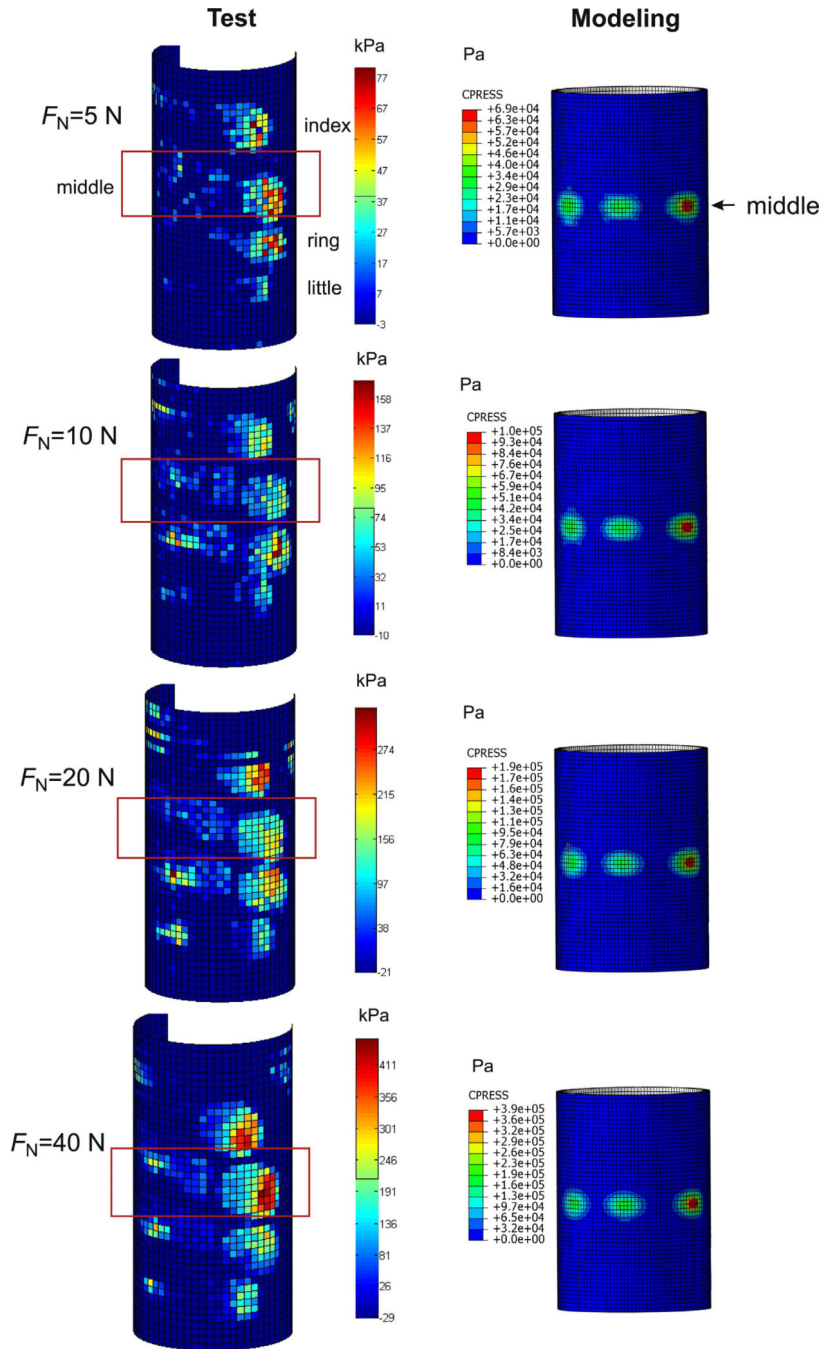


Fig. 3. Comparison of the contact pressure distributions measured experimentally with those simulated numerically. Left column: experimental measurements. Right column: model predictions. The contact pressures of four fingers (i.e., index, middle, ring, and little finger) were measured in the tests. Only the contact pressures on the middle finger, as framed, were used in the model calibrations. The contact pressure is defined as positive with RED indicating the highest magnitude. (For interpretation of the references to color in this figure legend, the reader is referred to the web version of the article.)

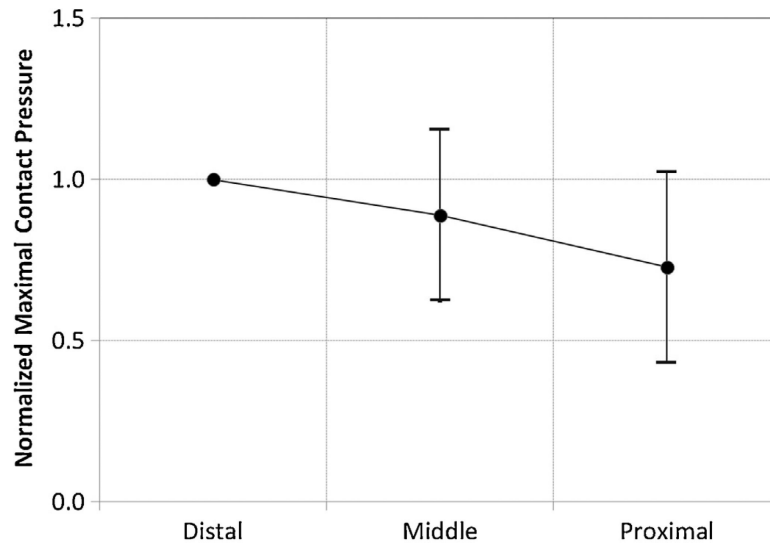


Fig. 4. The ratio of the maximal contact pressure on each segment of the middle finger. The maximal contact pressures on the middle and proximal segments are normalized to that on the distal segment. The data are the mean of the results of ten human subject tests.

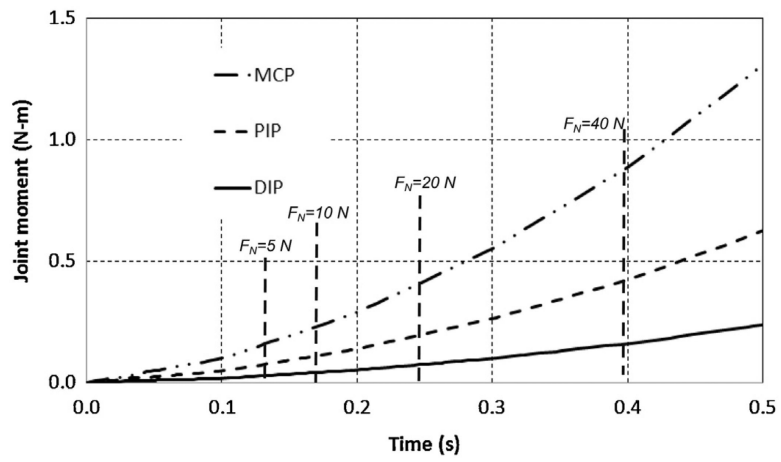


Fig. 5. The moments in the DIP, PIP, and MCP joints as a function of time. $F_N = 5\text{ N}$, $F_N = 10\text{ N}$, $F_N = 20\text{ N}$, and $F_N = 40\text{ N}$ represent the gripping forces applied in the tests (Fig. 3).

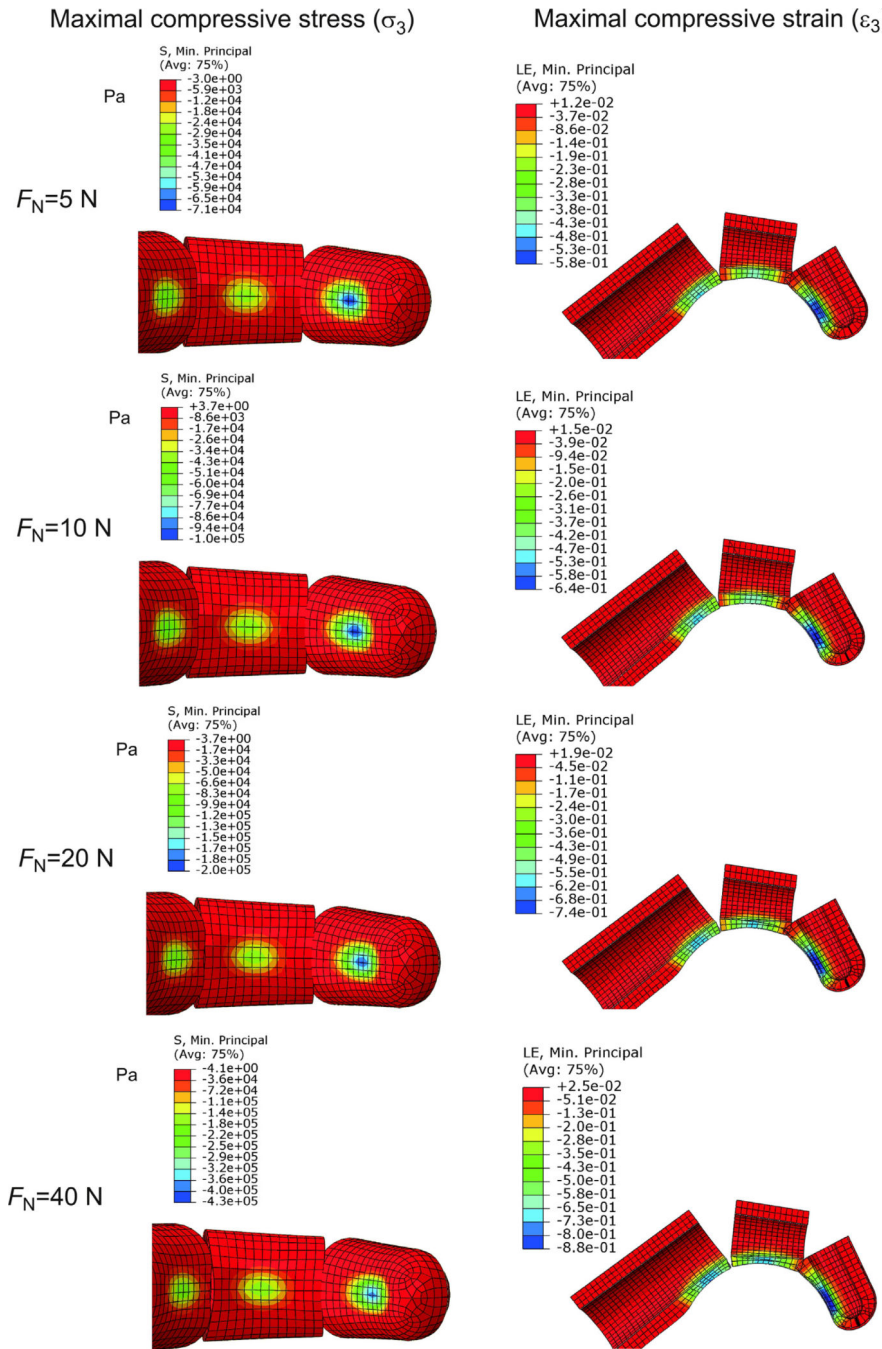


Fig. 6. The maximal compressive stress and strain in soft tissues as a function of the gripping force. Left column: the distributions of the maximal compressive stress on the skin surface of the distal, middle, and proximal segments. Right column: the distributions of the maximal compressive strains across the soft tissues of the distal, middle, and proximal segments. The compressive stress and strain are defined as negative with BLUE indicating the highest magnitude. (For interpretation of the references to color in this figure legend, the reader is referred to the web version of the article.)

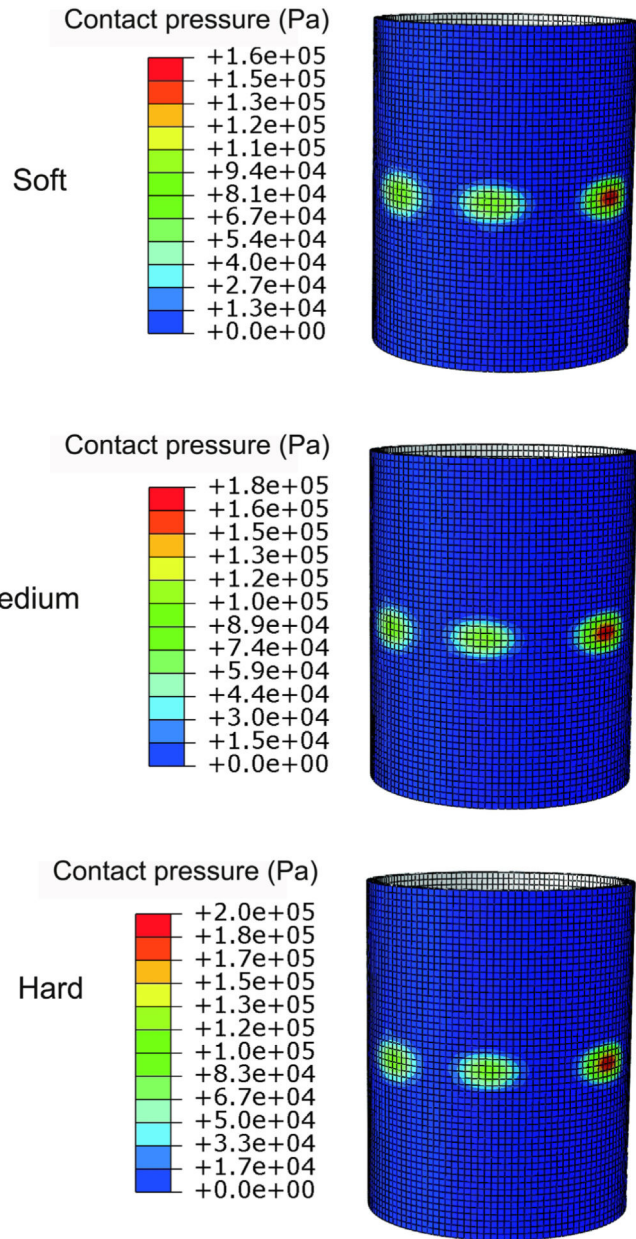


Fig. 7. The distributions of the contact pressure on the cylindrical handle covered with materials of three different stiffness levels. The contact pressure is defined as positive with RED indicating the highest magnitude. The mechanical properties of the covering materials, “Soft”, “Medium”, and “Hard”, have been evaluated and described in Appendix (Fig. A.1 and Table A.1). (For interpretation of the references to color in this figure legend, the reader is referred to the web version of the article.)

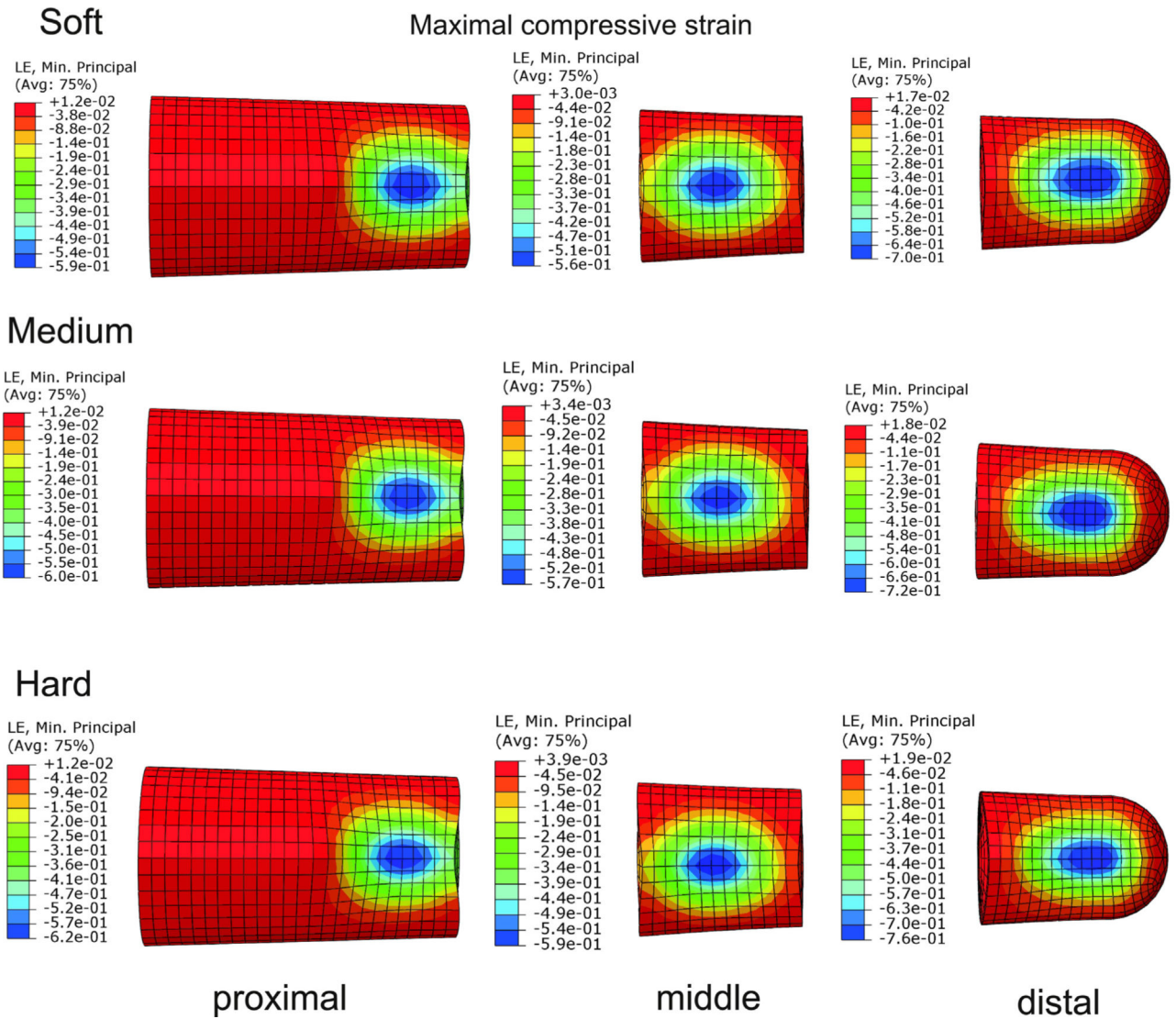


Fig. 9. The comparison of the maximal compressive strains on the skin surface of the distal, middle, and proximal segments for gripping a cylinder covered with materials of three different stiffness levels (“Soft”, “Medium”, and “Hard”). The magnitude of the maximal compressive strain in middle and proximal segments decreased with decreasing cover stiffness while that in the distal segment remained nearly constant. The compressive strain is defined as negative with BLUE indicating the highest magnitude. (For interpretation of the references to color in this figure legend, the reader is referred to the web version of the article.)

Table 1

The calculated maximal contact pressures at the distal, middle, and proximal finger segments for different contact force levels.

Grip force (N)	Contact pressure (kPa) Finger segment		
	Distal	Middle	Proximal
5	70	30	40
10	100	50	70
20	190	90	100
40	390	190	230

Author Manuscript

Author Manuscript

Author Manuscript

Author Manuscript